Electronic Supplementary Information (ESI)

Mechanistic understanding of microstructure formation during synthesis of metal oxide/carbon nanocomposites

Mennatalla Elmanzalawy,[1,2] Alessandro Innocenti,[1,2] Maider Zarrabeitia,[1,2] Nicolas J. Peter,[3] Stefano Passerini,[1,2,4] Veronica Augustyn,[5] Simon Fleischmann[1,2,*]

[1] Helmholtz Institute Ulm (HIU), 89081 Ulm, Germany
[2] Karlsruhe Institute of Technology (KIT), 76021 Karlsruhe, Germany
[3] Institute of Energy and Climate Research (IEK-2), Forschungszentrum Jülich GmbH, 52425 Jülich, Germany
[4] Department of Chemistry, Sapienza University of Rome, P. A. Moro 5, 00185 Rome, Italy
[5] Department of Materials Science & Engineering, North Carolina State University, Raleigh, NC 27606, USA
* Corresponding author's email: simon.fleischmann@kit.edu

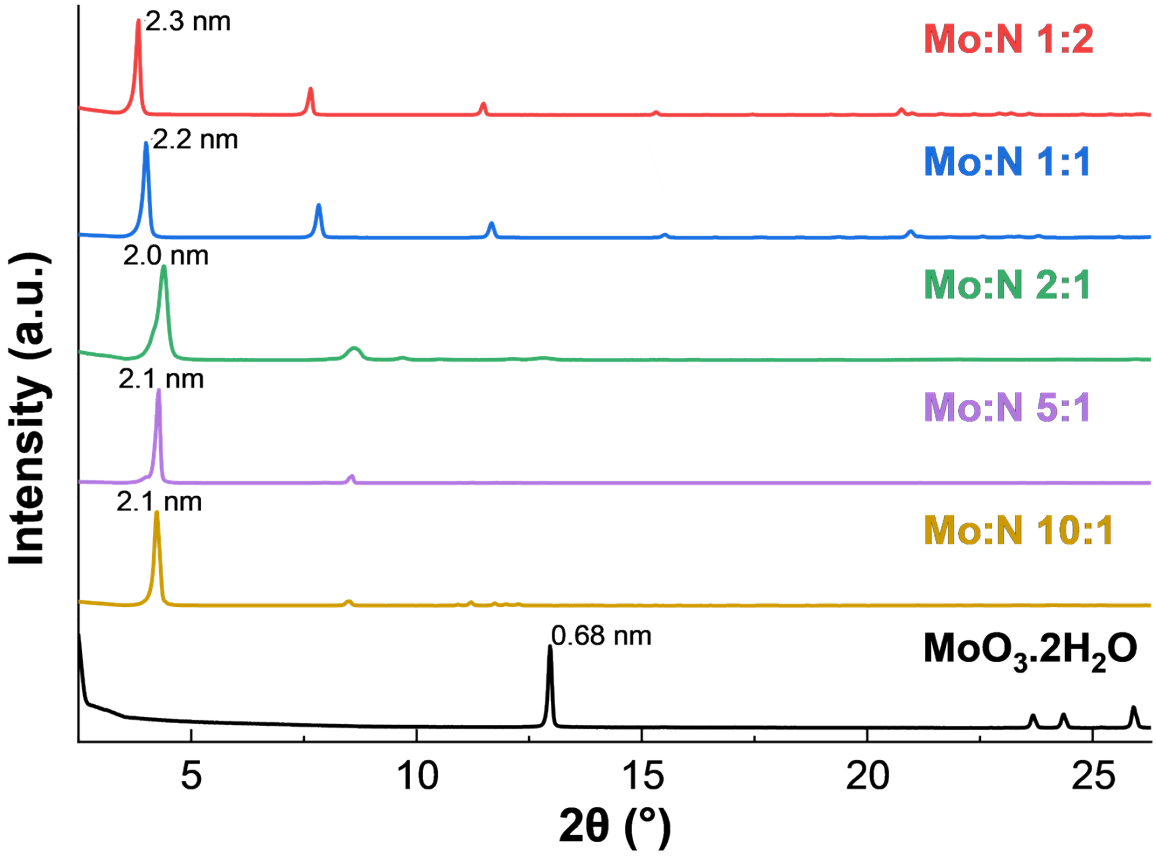

Fig. S1: XRD patterns of MoO_x-OA samples that were synthesized using various ratios of molybdenum oxide to octylamine.

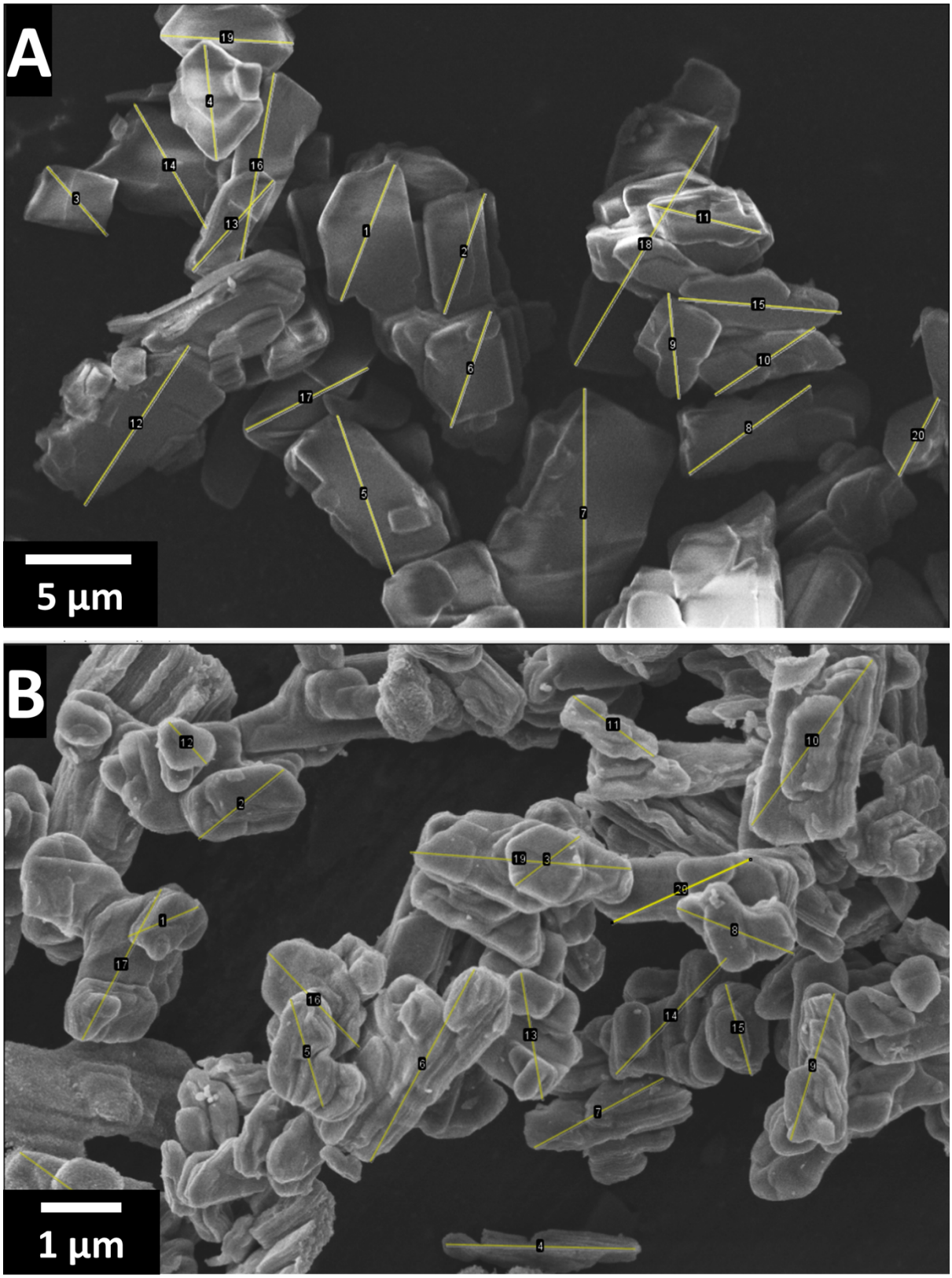

Fig. S2: SEM images used for the calculation of the average particle size of (A) MoO_x-OA and (B) MoO_x-C. A total of 20 particles were measured in each case.

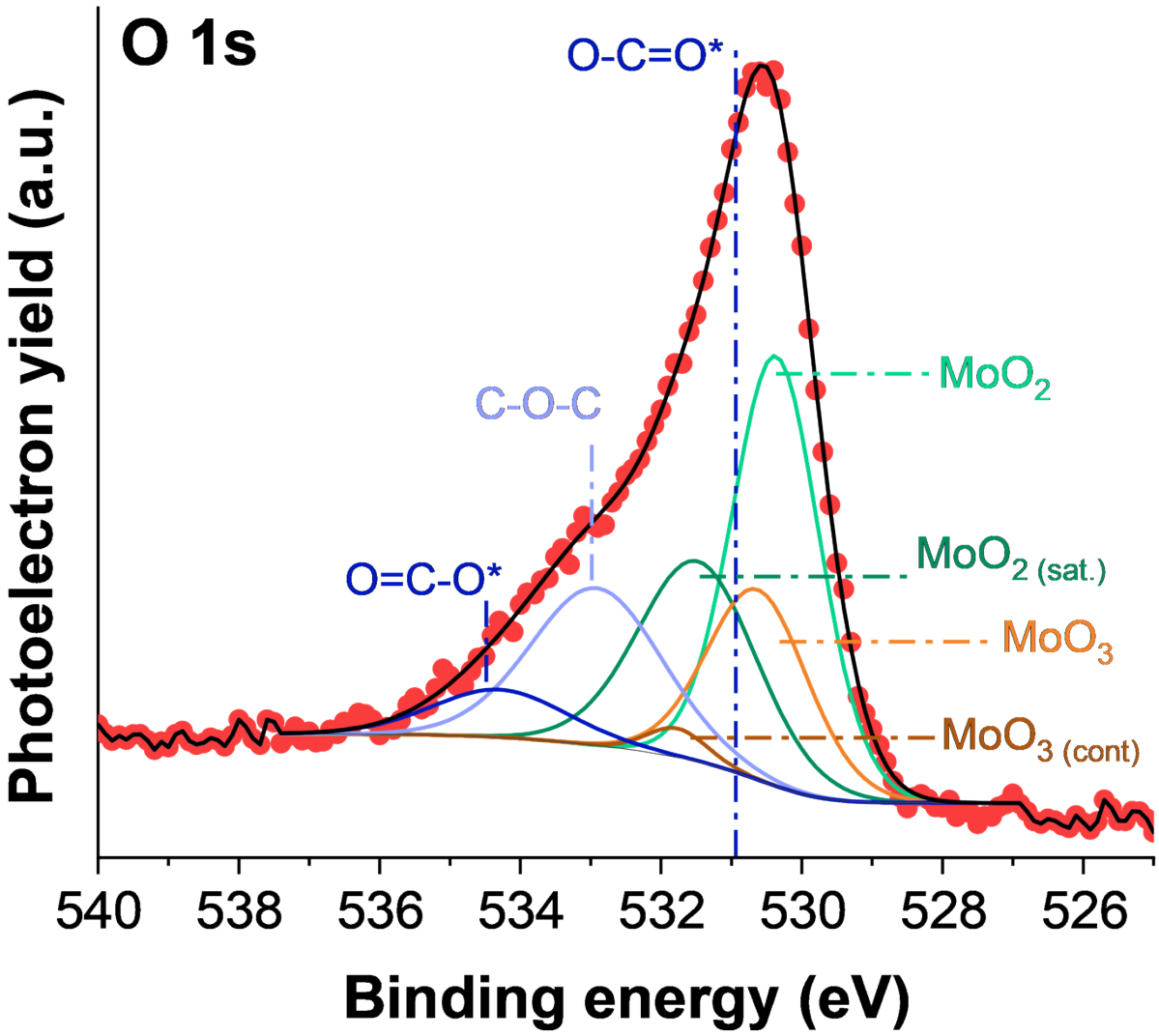

Fig. S3: O 1s XPS spectrum of pristine powder MoO_x-C, showing Mo(IV) oxide, Mo(VI) oxide, and carbon/oxygen species.[1,2]

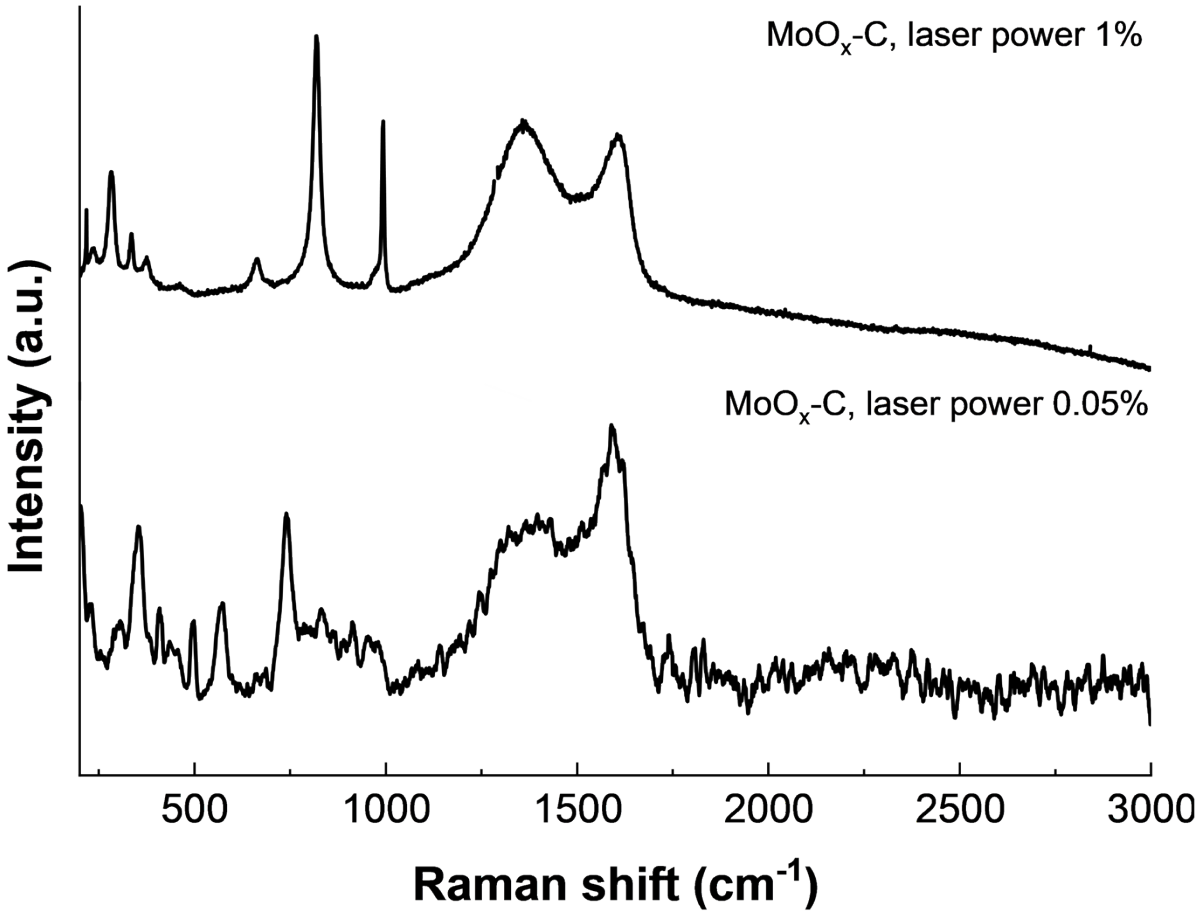

Fig. S4: Raman spectra of MoO_x-C acquired at 1 % (5 mW) and 0.05 % (0.25 mW) laser power, demonstrating the transformation from MoO_2 to MoO_3 signals at higher laser power.

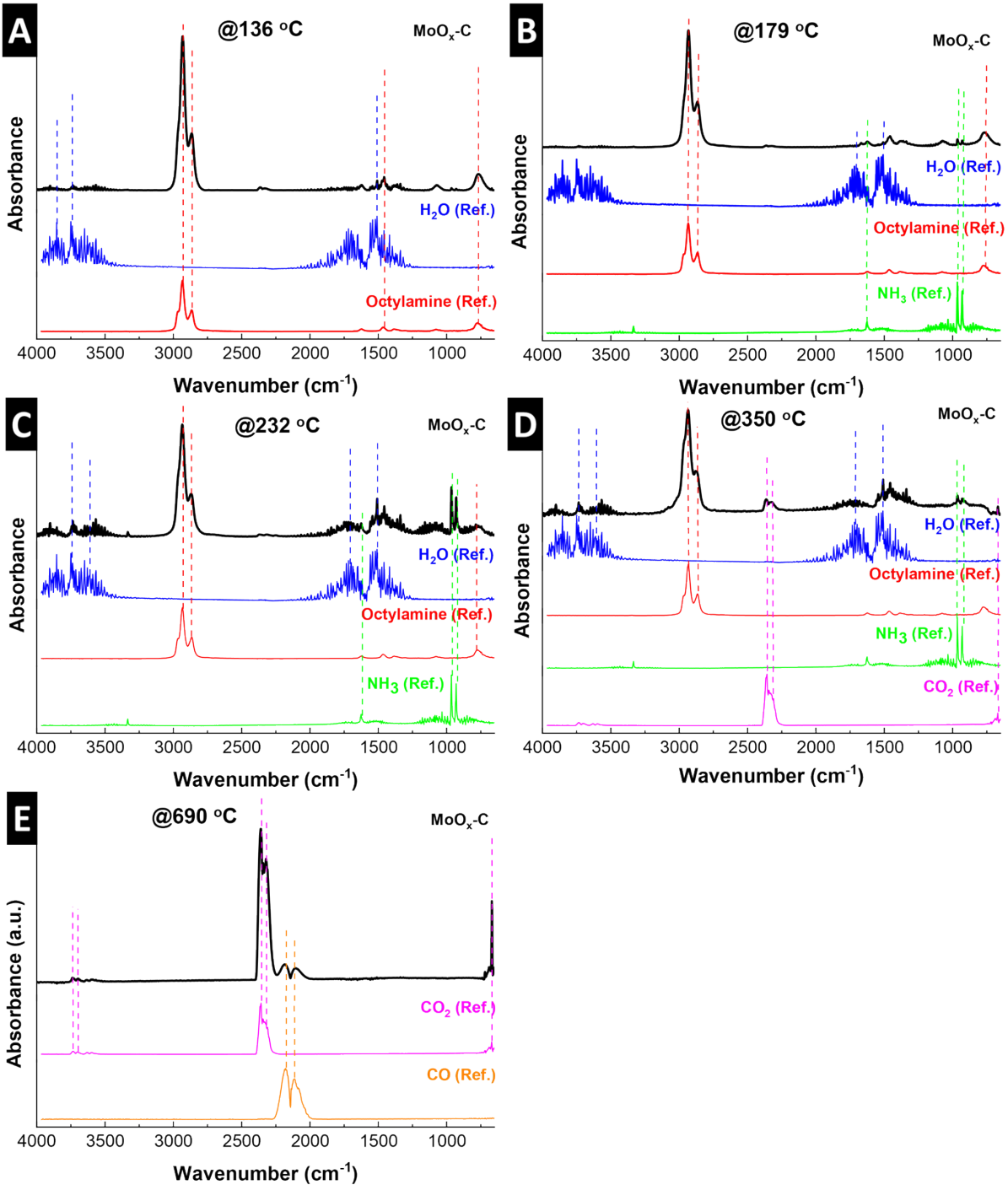

Fig. S5: FTIR spectra of the evolving gasses during pyrolysis in the TGA at selected temperatures, compared to typical referenced spectra of assigned molecules according to Ref.[3]

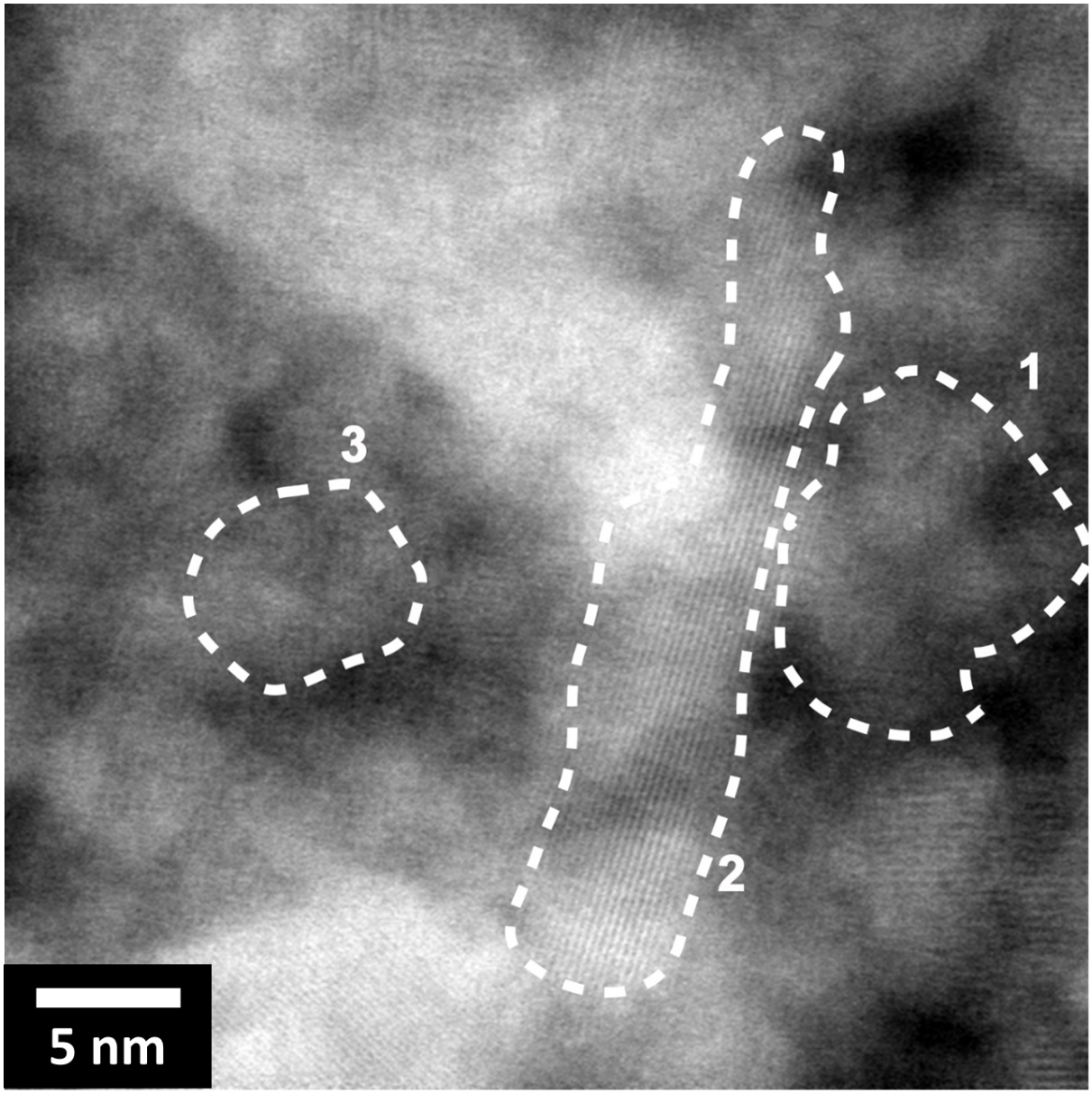

Fig. S6*: HAADF-STEM of MoO_x-C, corresponding to bright field image shown in Fig. 4C. The nanocrystalline domains are highlighted in regions 1, 2, and 3.*

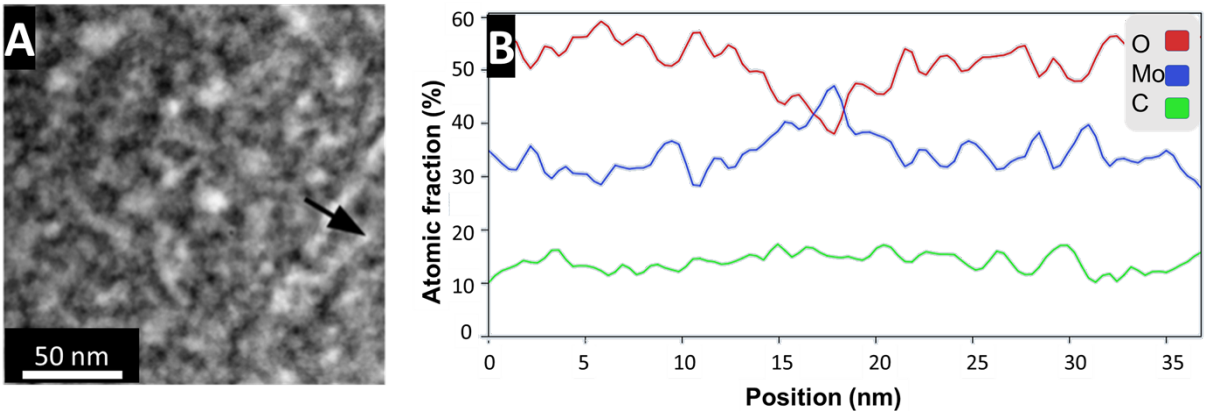

Fig. S7: A) STEM-HAADF image of MoO_x-C, B) EDS elemental profiles of O, Mo, and C across the arrow displayed in panel A. Since STEM-EDS is a semi-quantitative method due to peak overlap, chamber contamination, and X-rays emitted from the grid and sample holder, EDS line scanning was chosen instead of showing a discrete EDS spectrum at a specific location.

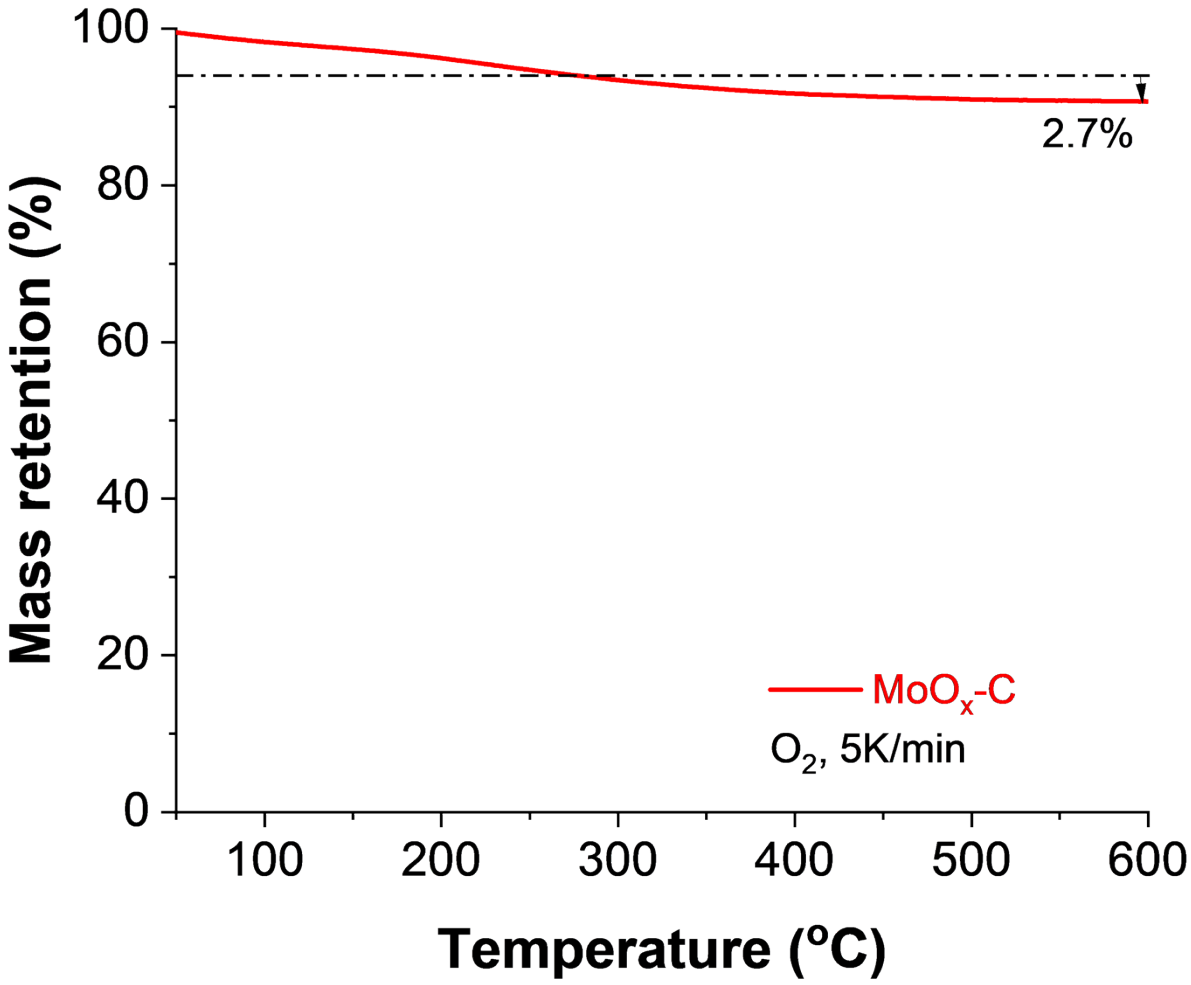

Figure S8: TGA of MoO_x-C heating in oxygen atmosphere. Start temperature for mass loss calculation was set to 300°C, since amorphous carbons start to burn off at ca. 320°C.[4]

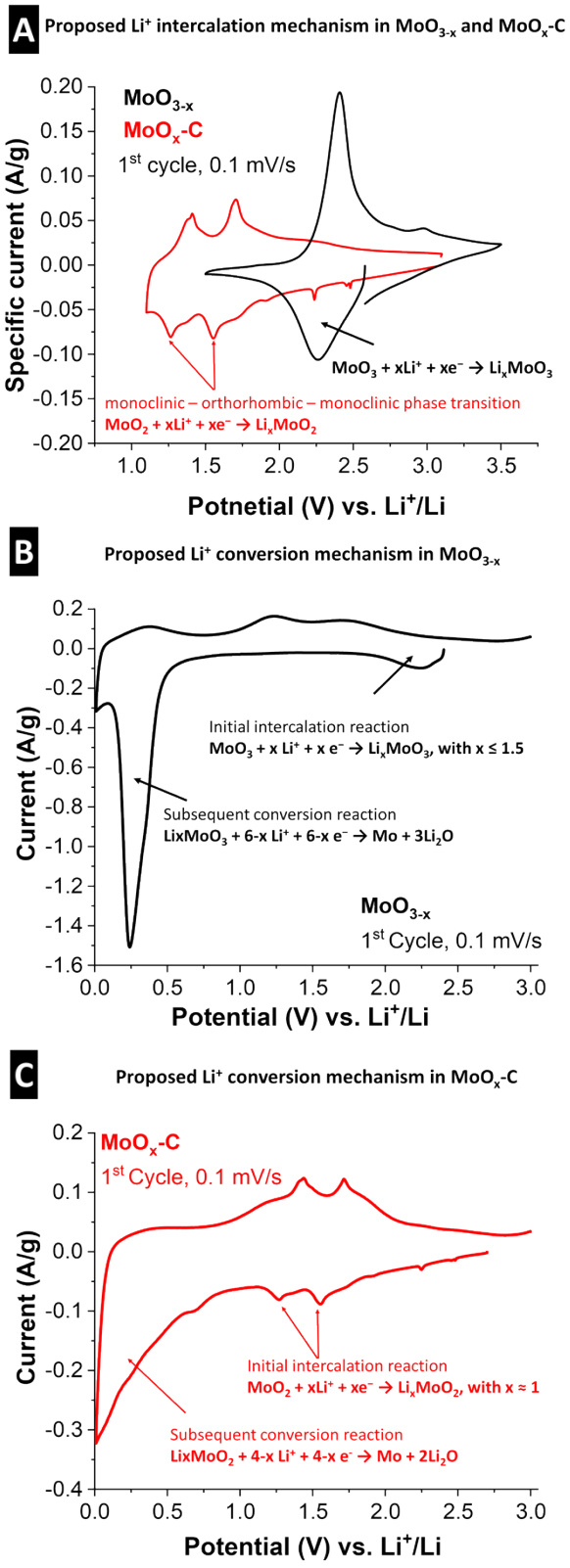

Fig. S9: *Cyclic voltammograms of MoO_{3-x} and MoO_x-C in the respective first cycle. (A) Within the lithium intercalation potential range and to extended negative potential of 0.01 V vs. Li^+/Li for (B) MoO_{3-x} and (C) MoO_x-C. The charge storage reactions for Li^+ intercalation and conversion reactions are annotated on the graphs.*

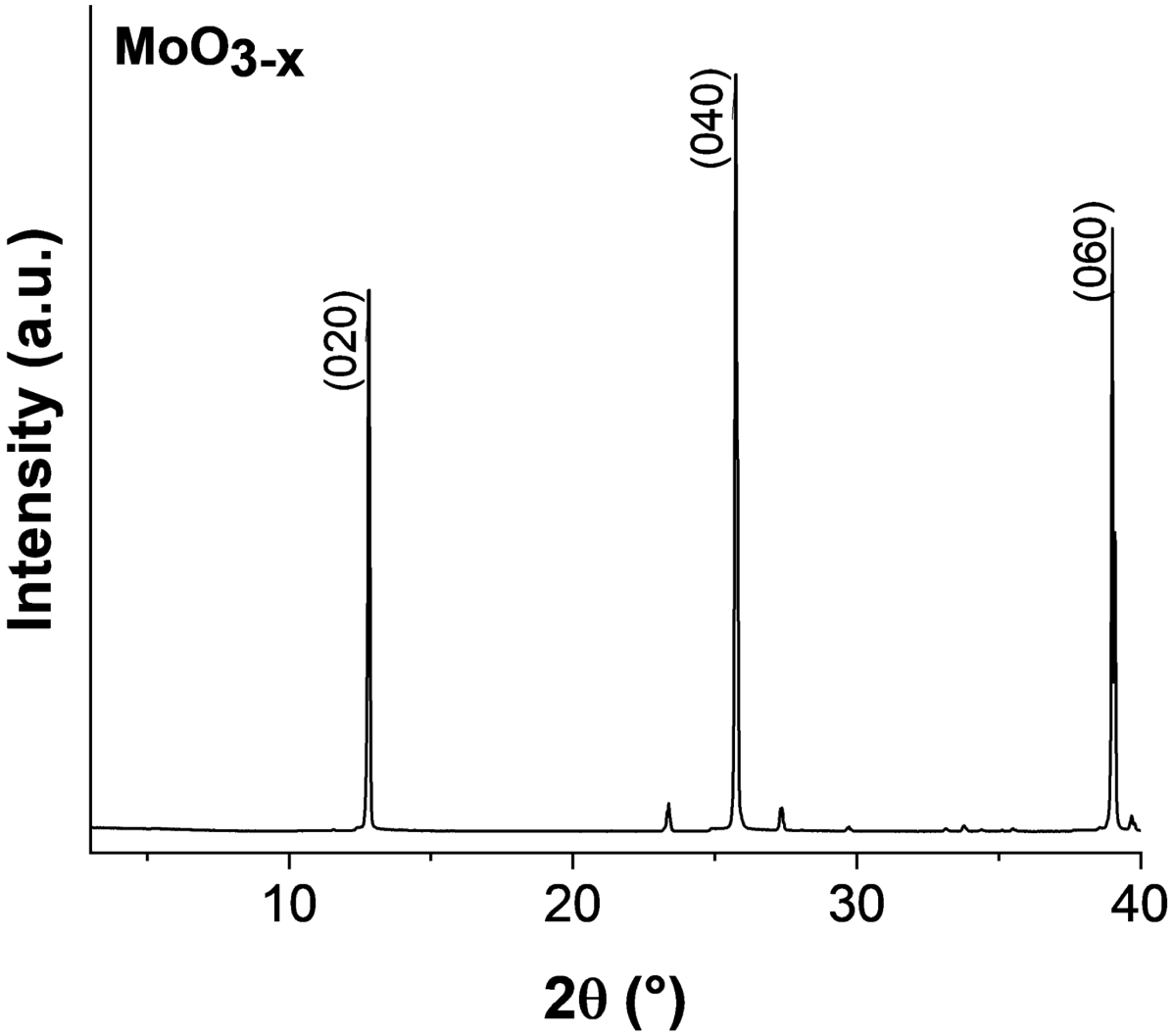

Fig. S10: XRD pattern of the as-synthesized reduced MoO_3, labelled in this work as MoO_{3-x}. The sharp (020), (040) and (060) diffraction peaks indicate preferred orientation along [0k0] direction, as described in ref. [5]

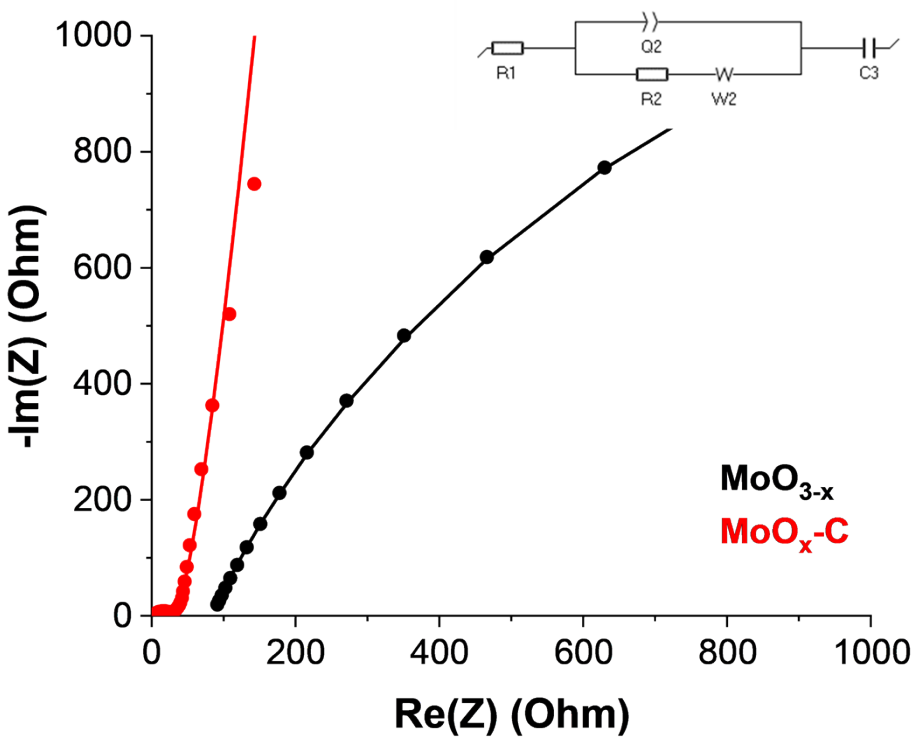

Fig. S11: Electrochemical impedance spectra of MoO_{3-x} and MoO_x-C performed at OCV. Solid lines represent the fitted curves obtained by the equivalent circuit in the inset, where R1 is the combined series resistance consisting of the ionic resistance of the electrolyte, the resistance of the active material, and the contact resistance at the electrode/current collector interface,[6] R2 is the charge transfer resistance, Q2 is the constant phase element (used to describe non-ideal capacitive behaviour from double-layer processes), W is the Warburg element (used to describe ion diffusion), and Q3 is the capacitance by faradaic processes, also referred to as limit capacitance.[7]

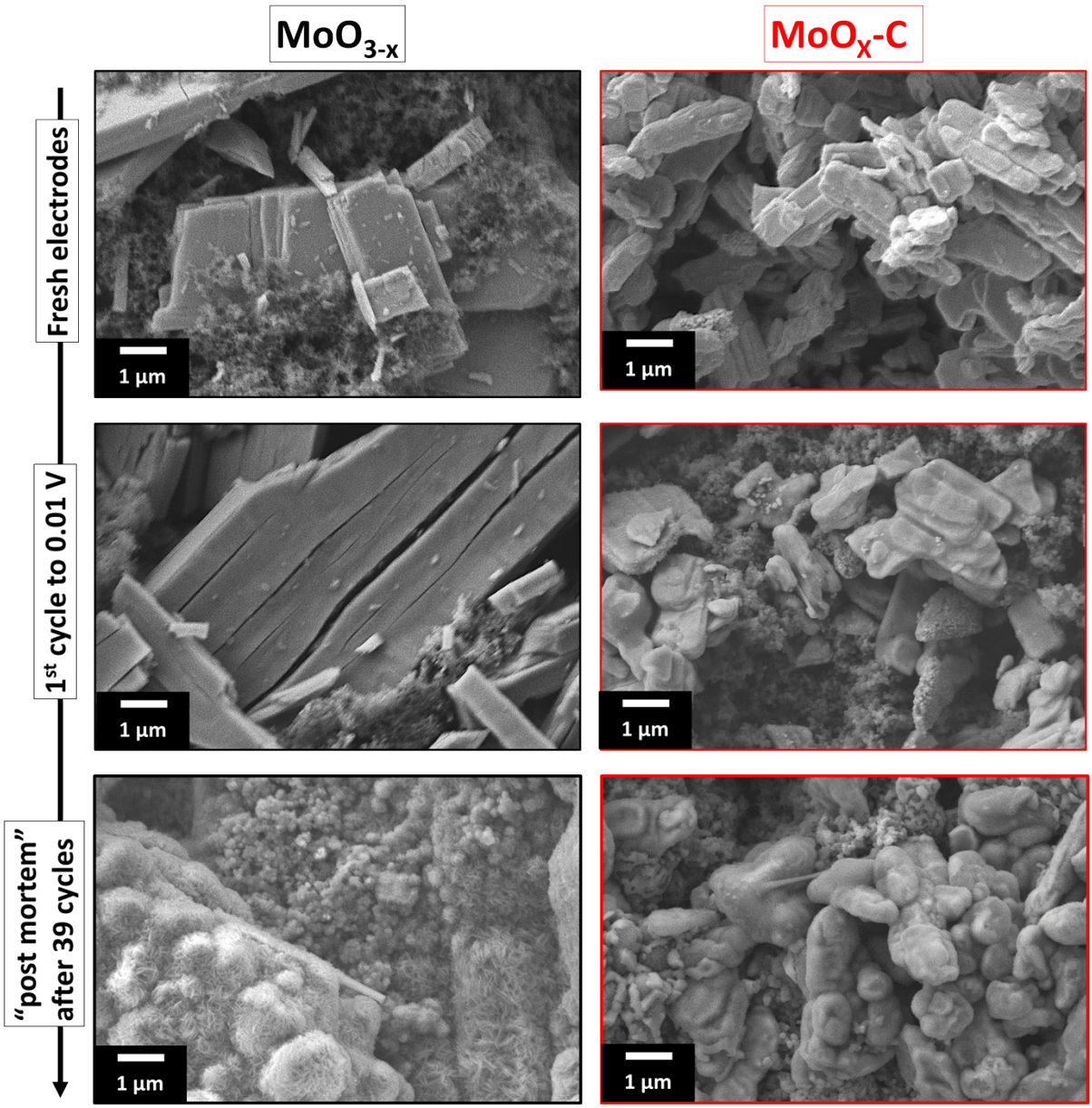

Fig. S12: SEM images of the pristine MoO_{3-x} (left column) and MoO_x-C (right column) electrodes (top), and ex situ SEM after the first electrochemical reduction to 0.01 V vs. Li^+/Li (center) and after galvanostatic cycling over 39 cycles (bottom).

References

(1.) Scanlon, D. O.; Watson, G. W.; Payne, D. J.; Atkinson, G. R.; Egdell, R. G.; Law, D. S. L. Theoretical and Experimental Study of the Electronic Structures of MoO 3 and MoO2. *Journal of Physical Chemistry C* **2010**, 114, 4636–4645.

(2.) Wagner, C. D.; Riggs, W. M.; Davis, L. E.; Moulder, J. F.; Muilenberg, G. E. *Handbook of X-Ray Photoelectron Spectroscopy*; Physical Electronics Division, Perkin-Elmer, Co.: Eden Prairie Minnesota, **1979**.

(3.) William E. Wallace. Infrared Spectra. In *NIST Chemistry WebBook, NIST Standard Reference Database Number 69*; Linstrom, P. J., Mallard, W. G., Eds.; National Institute of Standards and Technology: Gaithersburg MD.

(4.) Kim, K. S.; Imris, M.; Shahverdi, A.; Alinejad, Y.; Soucy, G. Single-Walled Carbon Nanotubes Prepared by Large-Scale Induction Thermal Plasma Process: Synthesis, Characterization, and Purification. *Journal of Physical Chemistry C* **2009**, 113, 4340–4348.

(5.) Kim, H. S.; Cook, J. B.; Lin, H.; Ko, J. S.; Tolbert, S. H.; Ozolins, V.; Dunn, B. Oxygen Vacancies Enhance Pseudocapacitive Charge Storage Properties of MoO3−x. *Nature Materials* **2016**, 16, 454–460.

(6.) Gamby, J.; Taberna, P. L.; Simon, P.; Fauvarque, J. F.; Chesneau, M. Studies and Characterisations of Various Activated Carbons Used for Carbon/Carbon Supercapacitors. *J. Power Sources* **2001**, 101, 109–116.

(7.) Kumar, S.; Rehman, M. A.; Lee, S.; Kim, M.; Hong, H.; Park, J. Y.; Seo, Y. Supercapacitors Based on Ti3C2Tx MXene Extracted from Supernatant and Current Collectors Passivated by CVD-Graphene. *Scientific Reports* **2021**, 11, 1–9.